Article

Combining spherical-cap and Taylor bubble fluid dynamics with plume measurements to characterize basaltic degassing

Tom D. Pering[1], Andrew J. S. McGonigle[1,2,3],

[1]   University of Sheffield, Department of Geography, Winter Street, Sheffield, UK; t.pering@sheffield.ac.uk
[2]   Istituto Nazionale di Geofisica e Vulcanologia, Sezione di Palermo, Via Ugo La Malfa, 153, 90146, Palermo, Italy.
[3]   School of Geosciences, The University of Sydney, NSW2006, Australia
*   Correspondence: t.pering@sheffield.ac.uk; Tel.: +44-1142-227961

Abstract: Basaltic activity is the most common class of volcanism on Earth, characterized by magmas of sufficiently low viscosities such that bubbles can move independently of the melt. Following exsolution, spherical bubbles can then expand and/or coalesce to generate larger bubbles of spherical-cap or Taylor bubble (slug) morphologies. Puffing and strombolian explosive activity are driven by bursting of these larger bubbles at the surface. Here, we present the first combined model classification of spherical-cap and Taylor bubble driven puffing and strombolian activity modes on volcanoes. We furthermore incorporate the possibility that neighboring bubbles might coalesce, leading to elevated strombolian explosivity. The model categorizes behavior in terms of the temporal separation between the arrival of successive bubbles at the surface and bubble gas volume or length, with the output presented on visually intuitive two-dimensional plots.   The categorized behavior is grouped into the following regimes: puffing from a) cap bubbles; and b) non-overpressurised Taylor bubbles; and c) Taylor bubble driven strombolian explosions; each of these regimes is further subdivided into scenarios whereby inter-bubble interaction does/doesn't occur. The model performance is corroborated using field data from Stromboli (Aeolian Islands, Italy), Etna (Sicily, Italy) and Yasur (Vanuatu), representing one of the very first studies, focused on combining high temporal resolution degassing data with fluid dynamics, as a means of deepening our understanding of the processes which drive basaltic volcanism.

Keywords: strombolian, puffing, Taylor bubble, gas slug, spherical-cap bubble, basaltic volcanism

1. Introduction

Basaltic volcanism is characterized by magmas of low viscosity, ranging $10^1 - 10^4$ Pa s [1], which enable free flow of gas bubbles within the melt, in contrast to the behavior of more viscous silicic systems [2]. In basaltic magmas spherical bubbles are generated, following exsolution of gas from the melt [3]. These bubbles grow via diffusion, decompression based expansion or coalesce to form non-spherical bubbles, e.g., of spherical-cap morphology [4-6], which can transition into Taylor bubbles (also called gas slugs), which nearly span the conduit width, and are of length ≥ the conduit diameter (see Fig. 1 for further detail on the morphological characteristics of spherical-cap and Taylor bubbles) [4,7,8]. These distinct bubble morphologies give rise to a variety of potential classes of surface degassing activity, specifically: passive degassing of spherical bubbles [2]; puffing, from bursting of non-spherical bubbles or non-over-pressurized Taylor bubbles [9-11]; and explosions from over-pressurized Taylor bubbles [12-14]. The latter scenario is associated with strombolian volcanism, as manifested on the eponymous Stromboli volcano, e.g., [9,15], where the activity has been well characterised through measurements of the erupted gas masses, e.g., [11,16-18], and studies into the explosive dynamics, e.g., [19-21].

46   A number of other targets worldwide also exhibit strombolian volcanism, e.g., Yasur [22],
47   Villarica [23], Etna [24], and Pacaya [25]. Similarly, puffing activity on volcanoes has been well
48   studied, using video, thermal imagery and gas measurement approaches, particularly on Stromboli,
49   e.g., [10,11,26,27].

50
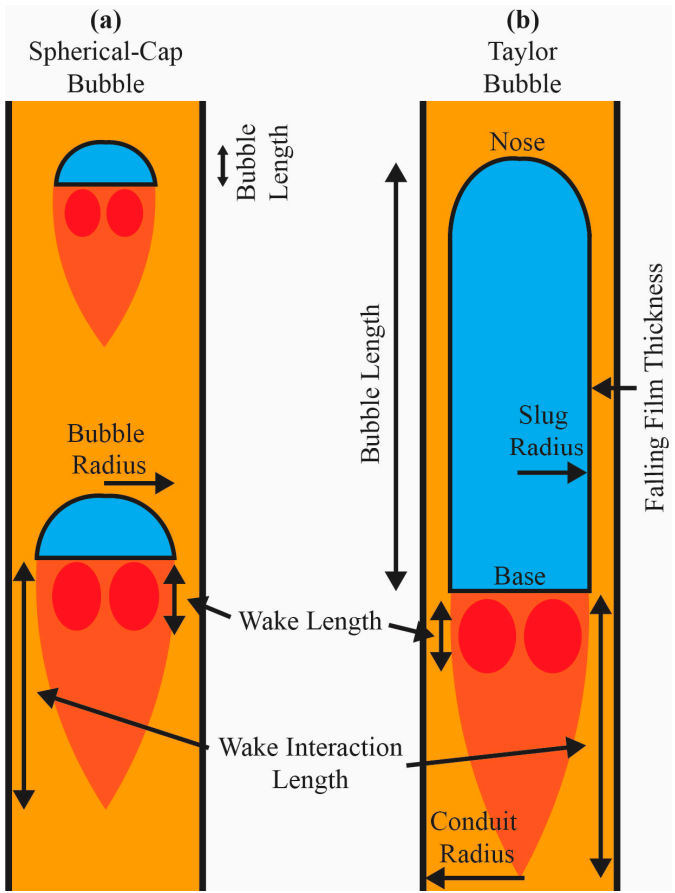
Figure 1. An illustration of (a) spherical-cap and (b) Taylor bubble morphologies including the bubble
features relevant to the model described here. Any bubble falling within the wake length of the bubble
ahead of it is considered liable for imminent coalescence. Any bubble beyond the interaction length
would be considered to flow independently (e.g., in the single regions of the model outputs shown in
Figs. 2 and 3). Bubbles within the interaction length are affected by the leading bubble (e.g., falling
within the rapid regions of Figs. 2 and 3).

57   Hitherto, considerable attention has been devoted to the fluid dynamics of discrete aspects of slug
58   flow on volcanoes, via mathematical, numerical and laboratory modelling approaches. In particular,
59   James et al. [13] investigated the evolution of Taylor bubble pressure and length during the ascent
60   process. Furthermore, James et al. [28] developed a criterion to quantify the transition between
61   puffing and explosive bursting, and Del Bello et al. [14] developed a static-pressure model for
62   bursting Taylor bubbles. However, to date there has been very little consideration of the fluid
63   dynamics of spherical-cap bubbles in a volcanic scenario, bar the work of Bouche et al. [29]. Spherical-
64   cap bubbles can be considered a transitionary morphology with characteristic shape (see Fig. 1), prior
65   to the formation of Taylor bubbles. These bubbles are characterised by a quasi-hemispherical nose
66   and horizontal base and, unlike slugs, have lengths ≤ the conduit width, and have yet to develop a
67   full falling film, as is the case with Taylor bubbles. There has also been very little attention devoted
68   to resolving the implications of inter-bubble interactions within these volcanic bubble flow regimes.
69   Recently we have highlighted the importance of coalescence between multiple rising Taylor bubbles,
70   in modulating the timing and intensity of high temporal resolution strombolian explosions, based on
71   field observations on Mt. Etna [24], and laboratory experiments [30]; the potential importance of this
72   phenomenon has also been highlighted by Gaudin et al. [26,27].

Here we present, for the first time, a combined model description, of the fluid dynamics of puffing and strombolian volcanism, driven by spherical-cap and Taylor bubbles. This has been achieved by: a) bringing together prior model treatments of individual aspects of Taylor bubble flow from the volcanic and fluid dynamics literature; b) considering, for the first time, spherical-cap bubbles in a volcanic scenario; and c) including the previously little considered (with notable exceptions including [31,32]) possibility that bubbles might interact with one another to coalesce and generate larger, e.g., more explosive masses. The model is also compared against degassing field data from Stromboli [11,17,18], Etna [24] and Yasur [33] volcanoes. This is one of the very first attempts to study volcanic degassing dynamics using a combination of modelling and gas flux time series [18], expedited by the advent of ≈1 Hz time resolution UV imaging of volcanic SO_2 fluxes which enables capture of rapid degassing phenomena in unprecedented detail [34-36]. This work is also one of only a few in recent years, focused on defining transitions between basaltic degassing modes, building on pioneering work performed in this area a number of decades ago, e.g., [37], that of Palma et al. [38] who identified the relationship between bubble bursting strength and duration of the styles of basaltic volcanic activity relevant to this study, and the more recent work of Gaudin et al. [26] who categorized explosions based on bubble sizes and eruptive properties.

2. Modelling transitions between spherical, non-spherical and Taylor bubble flow regimes

The model classifies strombolian and puffing degassing regimes as distinct areas on plots of inter-bubble burst spacing vs. bubble volume; this is illustrated schematically in Fig. 2. In particular, the activity is categorized within the following classes: puffing from spherical-cap bubbles; puffing from Taylor bubbles; and Taylor bubble driven strombolian explosions. There is also a further subdivision of these classes into scenarios whereby the bubbles can/cannot interact with one another, i.e., "single" and "rapid" bursting regimes, and a region where bubble coalescence would inhibit the presence of independent bubbles. The model (available as an Excel Spreadsheet) is contained within the supplementary material, with the underlying mathematics detailed below. In this section, transitions between bubble morphologies will be considered, i.e., the zonation with respect to bubble volume and length. In the following sections, the categorization in terms of inter-bubble spacing will be covered, specifically in terms of when inter-bubble interactions may occur.

Firstly, the degassing regimes are classified according to bubble volume (note that volume and length here are interchangeable using the formula for the volume of a cylinder, assuming a quasi-cylindrical geometry, and that data on bubble volume are often more readily acquirable than bubble lengths). Bubbles in basalts cease to act as spherical bubbles (e.g., following Stokes law) at low Reynolds numbers (Re_b), e.g., <0.3 [39], such that:

$$Re_b = \frac{\rho_m u_{sb} l}{\mu} \qquad \text{(Eq. 1)}$$

where ρ_m is the melt density, μ the melt viscosity, l the bubble length and u_{sb} is the spherical bubble rise speed, from Stokes law:

$$u_{sb} = \frac{2(\rho_m - \rho_g)g\left(\frac{l}{2}\right)^2}{\mu} \qquad \text{(Eq. 2)}$$

where ρ_g is the density of the gas phase and g gravitational acceleration. The l at which a bubble ceases to be spherical can therefore be defined, enabling demarcation of the length (i.e., bubble volume) at which non-spherical bubbles form in Fig. 2. Any bubbles smaller than this size would lead to passive degassing and effusive activity, for example from lava flows [40-42].
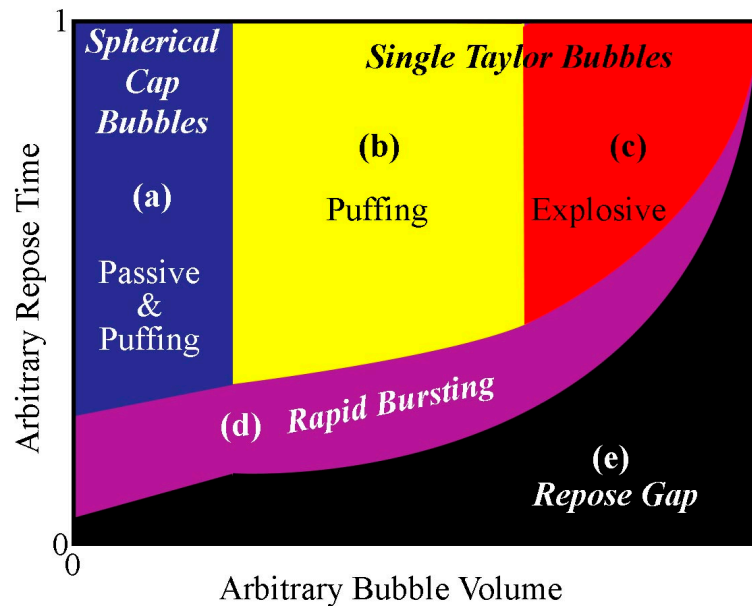
Figure 2. Illustrative example of the zonation between activity classes associated with the model, plotted on arbitrary inter-bubble repose time vs. bubble volume axes. Within area (a) are spherical-cap bubbles, which produce passive activity or light puffing, (b) and (c) are Taylor bubble flow scenarios resulting in non-explosive and explosively bursting scenarios, respectively. Area (d) represents cases where bubbles rise in sufficient proximity to one another to affect one another's fluid dynamics, while (f) corresponds to a region in which independent bubble bursting is unlikely due to coalescence between neighboring bubbles.

The non-spherical bubble regime is dominated by spherical-cap and Taylor bubbles, particularly at targets such as Stromboli, therefore our attention here will be focused on these bubble classes [5]. Spherical-cap bubbles burst passively at the magma surface or, as observed on Stromboli, can generate puffing, e.g., [10,11,19,26,27]. At larger bubble dimensions, spherical-cap bubbles transition into Taylor bubbles, when the bubble length exceeds that of the conduit diameter, e.g., [7]. Hence, areas are defined to the right of Fig. 2 relating to Taylor bubble driven activity involving puffing or strombolian explosions, depending on whether overpressure develops at the nose, e.g., [13]. This boundary has been defined by James et al. [28], who used the term, P^*_{slim}, which characterises burst vigour, and is ≥ 1 for explosive gas release. Here we adopt Eq. 13 from [28], to define this transition, for a Taylor bubble reaching the magma surface at a pressure equal to surface atmospheric pressure, P_{surf}, giving:

$$P^*_{slim} = 1 = \frac{\sqrt{\rho_m g A' l P_{surf}}}{P_{surf}} \qquad \text{(Eq. 3)}$$

where:

$$A' = 1 - \left(\frac{r_{TB}}{r_c}\right)^2, \qquad \text{(Eq. 4)}$$

such that: r_{TB} is the Taylor bubble radius, which is the conduit radius, e.g., r_c minus λ', where λ' is the thickness of falling film surrounding the Taylor bubble. The falling film thickness is found, as per Llewellin et al. [43], from:

$$\lambda' = 0.204 + 0.123\tanh(2.66 - 1.15\log_{10} N_f) \qquad \text{(Eq. 5)}$$

where the dimensionless inverse viscosity, N_f [7] is defined as:

151

$$N_f = \frac{\rho_m}{\mu}\sqrt{g(2r_c)^3} \qquad \text{(Eq. 6)}$$

152

153

154 Hence, following Eq. 3, the length, (and volume) at which slugs transition to explosive activity
155 can be determined. The second element of the model is to consider the significance of inter-bubble
156 spacing, in terms of determining whether spherical-cap and Taylor bubbles rise independently of one
157 another or whether interaction, which might lead to coalescence could occur. This is considered in
158 the following sections.
159

160 *2.1. Interactions between Taylor bubbles*

161

162 The ascent velocity of a Taylor bubble base u_{TB} is determined using the Froude Number, e.g.,
163 [43,44]:

164

$$Fr = 0.34\left[1 + \left(\frac{31.08}{N_f}\right)^{1.45}\right]^{-0.71} \qquad \text{(Eq. 7)}$$

166

167 such that:

168

$$u_{TB} = Fr\sqrt{2gr_c} \qquad \text{(Eq. 8)}$$

170

171 This speed is taken to be the average bulk rise velocity of a Taylor bubble [44] during ascent in
172 a volcanic conduit, as expansion, which causes acceleration of the nose, occurs closer to the surface
173 [13].
174 Other properties of Taylor bubbles are also important here, in particular, the wake length l_{wake},
175 and the wake interaction length l_{min}. The wake length, which is typically around four times shorter
176 than the wake interaction length, defines an area within which any trailing bubble will undergo near-
177 instantaneous coalescence with the leading Taylor bubble, as per [45]:

178

$$l_{wake} = 2r_c\left(0.30 + 1.22 \times 10^{-3}N_f\right). \qquad \text{(Eq. 9)}$$

180

181 The wake interaction length defines an area of fluidic disturbance beneath the Taylor bubble,
182 within which any following bubble will be affected by the leading Taylor bubble e.g., such that the
183 trailing bubble will no longer act independently [46]:

184

$$l_{min} = 2r_c(1.46 + 4.75 \times 10^{-3}N_f). \qquad \text{(Eq. 10)}$$

186

187 *2.2. Interactions between spherical-cap bubbles*

188

189 Spherical-cap bubbles can also be characterized in terms of Reynolds number, in this case
190 appropriate to the length scale of these bubbles. This scale is determined by the equivalent diameter,
191 d_e for bubbles of volume V_b [46]:

192

$$d_e = \left(\frac{6V_b}{\pi}\right)^{\frac{1}{3}}. \qquad \text{(Eq. 11)}$$

194

195 Such that the Reynolds number in this case is defined as follows [46]:

196

$$Re = \frac{\rho_m d_e u}{\mu}, \qquad \text{(Eq. 12)}$$

198

199 For u we use the ascent velocity of the Taylor bubble base (e.g., u_{TB}, to estimate the *Re* characteristics
200 of the system using a known velocity including effects of pipe diameter). The bubble drag coefficient
201 (C_d) is then calculated following [46]:
202

$$C_d = \left(2.67^{0.9} + \frac{16^{0.9}}{Re}\right)^{1.1} \qquad \text{(Eq. 13)}$$

204

205   This relationship is applicable for regimes with Morton numbers > 4 x 10^{-3}, a condition satisfied
206 in volcanic scenarios, e.g., [14]. Spherical-cap bubble rise velocity (u_{CB}) can then be calculated using
207 the following relationship, rearranged from Joseph [47], Eq. 2.1:
208

$$u_{CB}^2 = \frac{\left(\frac{g d_e}{C_d}\right)}{4/3} \qquad \text{(Eq. 14)}$$

210

211   Coalescence between two spherical-cap bubbles occurs in the same manner as for Taylor bubbles
212 [6,48]. To consider this, d_e is firstly converted to bubble diameter (d_b) using the constant 0.57 [4],
213 which accounts for the non-spherical morphology of these bubbles:
214

$$d_b = \frac{d_e}{0.57} \qquad \text{(Eq. 15)}$$

216

217   The wake length of spherical-cap bubbles, c_{wake}, applicable for *Re* < 200 (e.g., appropriate to
218 basaltic systems) is then determined as per Komasawa et al. [48]. Firstly, using bubble volume, V_b,
219 we can calculate the volume of the wake [48]:
220

$$V_w = V_b Re^{0.66} \qquad \text{(Eq. 16)}$$

222

223 which is then used to determine the wake length, c_{wake} from the following relationship:
224

$$V_w = \left(\frac{\pi d_w^2}{4}\right) \times (c_{wake} - l_{CB}), \qquad \text{(Eq. 17)}$$

226

227 where, d_w is the maximum wake diameter, which is taken as d_b, and l_{CB} is the length of the cap
228 bubble (taken as d_b / 2) [48]. For spherical-cap interaction length (c_{min}), there is no available prior
229 modelling literature to refer to here, hence we take this to be four times greater than c_{wake}, as this is
230 the approximate scaling between wake and wake interaction lengths in the Taylor bubble case,
231 although, as spherical-cap bubble volume decreases the influence of the interaction length will also
232 decrease.
233

234 *2.3. Bubble interactions*
235

236   Using the theory presented in 2.1 and 2.2 a temporal inter-bubble separation, t_{min}, can be defined
237 as a function of bubble volume (i.e., length) below which it would be highly improbable for an
238 independent trailing bubble to burst at the surface. In this case, any following bubble would be
239 travelling within the leading bubble's wake, hence would be liable for imminent coalescence; t_{min} was
240 therefore taken to be equal to the rise time of the trailing bubble (i.e., the ascent velocity of the
241 spherical-cap or Taylor bubble) through a column of liquid of thickness equal to that of the leading
242 wake length (l_{wake} or c_{wake}) plus the height of fluid (l_{film}), arising from complete drainage of the
243 film surrounding the leading bubble, following each burst. The latter was constrained, in the case of
244 Taylor bubbles, from film volume, as a function of slug volume, i.e., height, with knowledge of film
245 thickness, as per Eq. 5. For spherical-cap bubbles, this was constrained from bubble volume and
246 conduit volume around the bubble (i.e., applying the formula for the volume of a cylinder, for given
247 conduit and/or bubble radii).
248

249
$$t_{min} = \frac{l_{film} + l_{wake}}{u_{TB}} \quad \text{or} \quad t_{min} = \frac{l_{film} + c_{wake}}{u_{CB}} \qquad \text{(Eq. 18)}$$

250

251 This therefore defines a region on Fig. 2 (e), where bubble bursts are significantly less likely to
252 occur, i.e., within this region, all trailing bubbles are likely to undergo near-instantaneous coalescence
253 with the leading bubble. This area is termed the "repose gap" region, following the terminology of
254 Pering et al. [24], who in a study of rapid bursting events on Mt. Etna noted an absence of large mass,
255 low repose time events, hypothesizing that this behavior was due to coalescence; this region is also
256 discussed in a modelling framework in Pering et al. [30].
257 We can also define the time, $t_{transition}$, below which adjacent rising bubbles cannot be
258 considered to behave independently (e.g., bubbles are located within the wake areas of those ahead
259 of them), such that:

260

261
$$t_{transition} = \frac{l_{film} + l_{min}}{u_{TB}} \quad \text{or} \quad t_{transition} = \frac{l_{film} + c_{min}}{u_{CB}} \qquad \text{(Eq. 19)}$$

262

263 These durations correspond to the time taken for a Taylor or spherical-cap bubble to rise through a
264 column of melt of height equal to that of the drained film plus the wake interaction length, l_{min} or
265 c_{min}, of the leading bubble (Fig. 2), and are based on the lengths or volumes of bubble in question.
266 Hence, this line subdivides the non-spherical bubble degassing classes in Fig. 2, into categories where
267 the bubbles can/cannot be considered as rising independently of one another, respectively. Note that
268 a single area is used to denote non-independent (i.e., rapidly bursting) Taylor and spherical-cap
269 bubbles (Fig. 2d), without segregation between explosive and non-explosive cases for Taylor bubbles,
270 as complexities associated with pressure differences in this regime could lead to cases where the P^*_{slim}
271 parameter would not apply.

3. Model application to target volcanoes and comparison with field data

273 The model was initiated with a range of Taylor and spherical-cap bubble volumes relevant to
274 the volcano scale, e.g., with corresponding bubble lengths ranging from the centimeter scale for
275 spherical-cap bubbles, to the order of meters for Taylor bubbles. We apply the model for conditions
276 appropriate to three target volcanoes: Stromboli, Etna, and Yasur, where field data concerning
277 puffing/strombolian explosive behavior are available with inter-event repose intervals on the order
278 of seconds to minutes. The model outputs, with field data overlain, are shown in Fig. 3. During bubble
279 ascent the overlying viscous magma acts to retard expansion, i.e., creating a gas overpressure. To
280 account for this phenomenon we applied the model of Del Bello et al. [14] for Taylor bubble data for
281 Etna and Stromboli, which provides estimates of gas overpressure at burst and resulting bubble
282 lengths as a function of magmatic and conduit parameters, from which burst volumes can be
283 extracted.
284 The schematic representation of the model in Fig. 2 necessarily applies sharp definitions to the
285 boundaries between defined degassing areas. In reality, there will be a degree of fuzziness around
286 these, as the model, of course provides a mathematical simplification of the 'real world' conditions
287 in volcanic conduits.

288

289
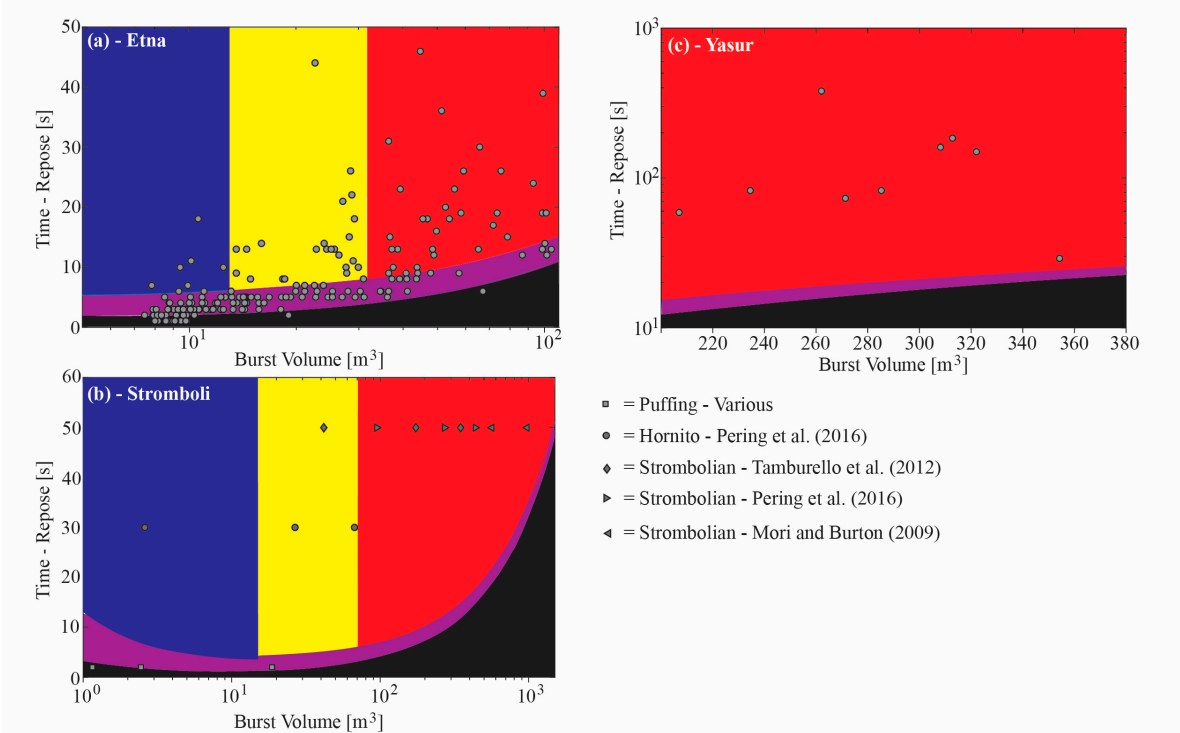
290 **Figure 3.** Outputs from the model run with input conduit and fluid dynamic parameters appropriate
291 to: (a) Mt. Etna; (b) Stromboli; and (c) and Yasur volcanoes. Overlain on the plots are data points
292 derived from field measurements on these targets, for Etna from Pering et al. [24] and Yasur from
293 Kremers et al. [33]. In the Stromboli case, a number of literature sources are referred to, as detailed
294 above. In each case a single repose interval is applied, which is a minimum for the observed activity.
295 Fig. 3b also just shows the maximum, mean and minimum burst volumes from each of Stromboli
296 papers, to simplify the graphic.

297   Firstly, we considered the case of Mt. Etna (Fig. 3a). Here we took UV camera field data from
298 Pering et al., [24], captured during a period of very rapid bubble bursting activity (modal inter-burst
299 period ≈ 4 s) observed at the Bocca Nuova crater. Here, observed masses were converted to in-conduit
300 volumes, using a pressure value of ≈ 65 kPa (i.e., for Mt. Etna's summit craters' altitude ≈ 3300 m)
301 within the Del Bello et al. [14] model. The parameters applied within our model were: magma density
302 of 2600 kg m^3, viscosity of 2000 Pa s, and conduit radius of 1.5 m, e.g., [49]. In general, the field data
303 clearly fall above the repose gap area, affirming the model suggestion from Pering et al. [24] that
304 independently bursting large volume, low repose time events would be improbable, due to inter-
305 bubble coalescence in the conduit. The majority of bursts (62%) fall within the rapid bursting Taylor
306 and spherical-cap bubble area, with 15% contained in the single Taylor bubble explosive area, 12% in
307 the single Taylor bubble puffing area, and most of the remainder in the single puffing area, indicative
308 of activity spanning the strombolian explosive-puffing spectrum. In the case of this rapid bursting
309 scenario, the model points towards bubble interaction playing a key role in the fluid dynamics, as
310 previously suggested by Pering et al. [24].
311   Secondly for Stromboli (Fig. 3b) we ran the model with density, viscosity and conduit radius
312 values of 2700 kg m^{-3}, e.g., [50,51], 300 Pa s, e.g., [52], and 1.5 m, respectively, e.g., [53,54]. Fig. 3b also
313 includes a range of field data points, based on literature derived main vent burst volumes [11,17,18].
314 These data generally fall within the single explosive Taylor bubble region, in line with the classical
315 strombolian activity associated with this target. However, the very smallest bursts from the
316 Tamburello et al. [11] dataset fall within the single Taylor bubble puffing region, capturing the
317 spectrum of activity exhibited at the volcano. For the specifically described 'puffing' events from
318 Tamburello et al. [11], all the data points are located away from the rapid Taylor bubble bursting area.
319 Note that in all the above cases, minimum repose times from the literature have been assigned, e.g.,

320   50 s from Ripepe et al. [10] for puffing. Hence, even for these rather extreme prescriptions of inter-
321   burst temporal resolution, the model points towards clearly independent bubble flow behaviour.
322   In addition, Pering et al. [18] reported on non-explosive puffing events, from a hornito adjacent
323   to the South-East crater, with a minimum repose interval of 30 s. These data fall within the single
324   puffing areas for Taylor and spherical-cap bubbles. Even smaller decimetre sized bubbles have also
325   been associated with puffing activity from smaller vent openings at Stromboli with repose intervals
326   of ≈ 0.5 – 2 s [9,10]. When plotted on Fig. 3b, these events mostly lie in the rapid puffing area of the
327   model, in view of their rather smaller inter-event durations than those puffing events reported in
328   Pering et al. [18].
329   Thirdly, the model was run for Yasur volcano (Fig 3c). Here, Kremers et al. [33] reported on
330   infrasonic observations of Taylor bubble bursting, quoting slug lengths and inter-event intervals for
331   a number of events. Here, we applied magma density and viscosity values of 2600 kg m^3 and 1000 Pa
332   s, with a conduit radius of 1.5 m [22] within the model. In particular, we converted the Kremers et al.
333   [33] data to volume (see Table 1) using the formula for the volume of a cylinder (the infrasound
334   derived length data in Kremers et al. [33] already account for pressure and viscous effects), and plot
335   against repose time in Fig. 3c. In this case all data fall within the single explosive Taylor bubble region,
336   in line with the existent strombolian activity, and indicating independent bubble flow, well outside
337   the repose gap region.
338

339   **Table 1.** Slug length and repose time data associated with rapid strombolian activity on Yasur volcano
340   (Kremers et al., [33] Table 2) in addition to calculated explosive gas volumes.

Length (m)	Volume (m³)	Repose (s)
118.5	285	82
174.9	354	29
138.5	308	160
68.6	207	59
109.7	271	73
149.5	322	149
142.1	313	185
102.6	262	380
83.7	235	82

341

342   4. Discussion and Limitations

343   Here, we present the first unified fluid dynamic treatment of spherical-cap and Taylor bubble driven
344   puffing and strombolian explosive activity in basaltic volcanism, the most ubiquitous class of activity
345   on Earth. This involves concatenation of discrete modelled aspects of Taylor bubble flow in volcanic
346   scenarios, the consideration of spherical-cap bubble fluid dynamics in volcanology (building on the
347   considerations of [29]), and incorporation of the possibility of inter-bubble interaction, which has
348   been little considered, hitherto. We also compared the model against field data from Etna, Stromboli
349   and Yasur volcanoes, resulting in the field data falling as would be expected within the areal zonation
350   of activity regimes, e.g., in respect of whether strombolian activity or puffing was manifested. In
351   particular, the general absence of data points in the repose gap region of the plots, affirmed the
352   expectation that bubble-coalescence would mitigate against independent bubble bursting in this area.
353   A further model success is the seamless flow between the c_{min} and l_{min} traces, i.e., the transition
354   between Taylor and spherical-cap regions. Hence, the mathematical treatments presented here
355   appear not to break down close to this regime shift. The flow between c_{wake} and l_{wake} for the Etna
356   data (Fig 3a) demonstrates similar seamlessness, however, there is a slight mismatch for the Stromboli

357 data (Fig. 3b), highlighting a need for further study into interaction lengths of spherical-cap bubbles.
358 In this treatment, we assume that rapid strombolian activity, such as that observed at Etna are driven
359 by trains of fully formed gas slugs, with associated fluid dynamic features, for the duration of ascent
360 from depth prior to burst.
361   Whilst a few data fell slightly within the repose gap region of Fig. 3a and 3b, this is likely
362 explicable by the following: a) The repose gap region refers to an area where bursting is improbable,
363 rather than impossible, and is based on the assumption that a bubble cannot exist independently
364 within the wake of another bubble; in reality such a bubble would have a very short, yet finite,
365 lifetime which could account for the slight overlap of some data into the repose gap region, and is
366 commensurate with the close proximity of all such events to the transition line; b) for the Etna data,
367 all such events are within a second of the repose gap line, which is likely at least partially a result of
368 the margin of error of the inter-event durations, given the quantized camera acquisition time stamp
369 and finite exposure times (100s of ms); c) for the Stromboli data, the very smallest puffing events from
370 Ripepe et al. [10] fall within the repose gap, potentially indicating that this activity is associated with
371 somewhat different magmatic and rheological properties than those reported in the literature for the
372 bulk conduit conditions of Stromboli, and assigned to the model. Alternately, this could indicate that
373 our assumption that c_{min} is four times c_{wake}, based on the behaviour of Taylor bubbles, could be an
374 overestimate; d) a final issue is that the model does not include complexities associated with the flow
375 of bubble trains. Here, all bubble ascent velocities have been based on models associated with the
376 flow of single bubbles in vertical conduits. In fact, in bubble trains rise velocities are higher than in
377 the single bubble case [55-57], and there is also the issue of near-surface of expansion of trailing
378 bubbles, e.g., [13]. Both of these effects will act to lower the c_{min}, c_{wake}, l_{min} and l_{wake} traces in Figs.
379 2 and 3, plausibly also accounting for the very few data points that fell within the repose areas of the
380 Etna and Stromboli plots. Future model development could take into consideration these effects, in
381 addition to inclusion of more complex and realistic conduit conditions, e.g., [12] such as inclination
382 [58,59] and formation of viscous caps at the top of the conduit [26,60], both of which are possibilities
383 on Stromboli.

384

385 **5. Conclusions**

386   Here, we present the first unified model treatment of cap bubble and slug based puffing and
387 strombolian explosive degassing behaviour in volcanoes. This model illustrates the exciting new
388 scientific frontiers expedited by the recent advent of high speed imaging of volcanic gas plumes, such
389 that models for subterranean fluid dynamics can be corroborated with surface degassing
390 observations [61] in far more detail than possible previously with then available temporally coarser
391 degassing data. Indeed, this work is one of the very first to exploit this opportunity, following on
392 from Pering et al. [18,24]. In particular, this framework offers the possibility of diagnosing
393 underground fluid dynamic, conduit or magmatic conditions, based on surface observations of burst
394 masses and timings. Future work could focus on augmenting this combined UV camera to model
395 development framework with contemporaneous in-situ gas composition data [62,63], and infrasound
396 measurements [25].
397   This work is also focused on defining fluid dynamic transitions between disparate basaltic
398 degassing classes, highlighting the key role played by inter-bubble separation and coalescence during
399 such activity. There has been very little work in this area since seminal research, e.g., [37] a number
400 of decades ago. This new capacity to develop models, informed by high time resolution UV camera
401 observations offers exciting promise to provide step change advances in this field, extending to a
402 wider range of basaltic styles, e.g., covering hawaiian activity. In particular, at basaltic volcanoes such
403 as Mt. Etna, where activity styles can transition rapidly between puffing and passive degassing
404 through single strombolian explosions to more rapid bursting events, and finally to hawaiian lava
405 fountaining [62,63], the model could be of utility in eruption forecasting.

406

6. Notation and Greek Letters

This section contains the notation and Greek letters used throughout this manuscript (listed in appearance order). Units used, where applicable, are included in brackets.

Re_b = Bubble Reynolds number

ρ_m = Magma density (kg m^3)

u_{sb} = Ascent velocity of a spherical bubble (m s^{-1})

l = Bubble length (m)

μ = Magma viscosity (Pa s)

ρ_g = Gas density (kg m^3)

g = Gravitational acceleration (m s^{-2})

P^*_{slim} = Dimensionless burst vigour

A' = Ratio of bubble radius to pipe radius

P_{surf} = Atmospheric pressure at the surface (Pa)

r_{TB} = Taylor bubble radius (m)

r_c = Conduit radius (m)

λ' = Falling film thickness (m)

N_f = Dimensionless inverse viscosity

Fr = Froude number

u_{TB} = Taylor bubble base ascent velocity (m s^{-1})

l_{wake} = Taylor bubble wake length (m)

l_{min} = Taylor bubble interaction length (m)

d_e = Equivalent diameter (m)

V_b = Bubble volume (m^3)

Re = Reynolds number

C_d = Bubble drag coefficient

u_{CB} = Spherical cap bubble base ascent velocity (m s^{-1})

d_b = Bubble diameter (m)

V_w = Volume of spherical cap bubble wake (m^3)

c_{wake} = Spherical cap bubble wake length (m)

l_{CB} = Cap bubble length (m)

c_{min} = Spherical cap bubble interaction length (m)

t_{min} = Minimum repose time (s)

$t_{transition}$ = Transition time (s)

Author Contributions: T.D.P designed and implemented the described model. T.D.P and A.J.S.M wrote the manuscript.

450   **Conflicts of Interest:** The authors declare no conflict of interest.

451   **References**

452   1.   Shaw, H.R.; Wright, T.L.; Peck, D.L.; Okamura, R.R. The viscosity of basaltic magma; an analysis of field
453   measruements in Makaophui lava lake, Hawaii. *Am. J. Sci.* **1968**, *266*, pp. 225-264,
454   DOI:10.2475/ajs.266.4.225

455   2.   Parfitt, E.A. A discussion of the mechanisms of explosive basaltic eruptions. *J. Volcanol. Geotherm. Res.* **2004**,
456   *134*, pp. 77-107, DOI:10.1016/j.jvolgeores.2004.01.002

457   3.   Sparks, R.S.J. The dynamics of bubble formation and growth in magmas: A review and analysis. *J. Volcanl.*
458   *Geotherm. Res.* **1978**, *3*, pp. 1-37, DOI:10.1016/0377-0273(78)90002-1

459   4.   Davies, R.M.; Taylor, G.I. The mechanics of large bubbles rising through extended liquids and through
460   liquids in tubes. *Proc. R. Soc. London, A.* **1950**, *A200*, pp. 375-390, DOI:10.1098/rspa.1950.0023

461   5.   Wegener, P.P.; Parlange, J. Spherical-cap bubbles. *Annu. Rev. Fluid Mech.* **1973**, *5*, pp. 79-100

462   6.   Bhaga, D.; Weber, M.E. Bubbles in viscous liquids: shapes, wakes, and velocities. *J. Fluid Mech.* **1981** *105*,
463   61-85

464   7.   Wallis, G.B. *One-dimensional two-phase flow*, McGraw-Hill: New York, USA, **1969**

465   8.   Morgado, A.O.; Miranda, J.M.; Araújo, J.D.P.; Campos, J.B.L.M. Review on vertical gas-liquid slug flow.
466   *Int. J. Multiph. Flow.* **2016**, *85*, pp. 348-368, DOI:10.1016/j.ijmultiphaseflow.2016.07.002

467   9.   Ripepe, M.; Gordeev, E. Gas bubble dynamics model for shallow volcanic tremor at Stromboli. *J. Geophys.*
468   *Res.* **1999**, *104*, pp. 10,639-10,654, DOI:10.1029/98Jb02734

469   10. Ripepe, M.; Harris, A.J.L.; Carniel, R. Thermal, seismic and infrasonic evidences of variable degassing rates
470   at Stromboli volcano. *J. Volcanol. Geotherm. Res.* **2002**, *118*, pp. 285-297, DOI:10.1016/S0377-0273(02)00298-6

471   11. Tamburello, G.; Aiuppa, A.; Kantzas, E.P.; McGonigle, A. J. S.; Ripepe, M. Passive vs. active degassing
472   modes at an open-vent volcano (Stromboli, Italy). *Earth Planet. Sci. Lett.* **2012**, *359-360*, pp. 106-116,
473   DOI:10.1016/j.epsl.2012.09.050

474   12. Seyfried, R.; Freundt, A. Experiments on conduit flow and eruption behaviour of basaltic volcanic
475   eruptions. *J. Geophys. Res.* **2000**, *105* , pp. 23,727-23,740, DOI:10.1029/2000JB900096

476   13. James, M.R.; Lane, S.J.; Corder, S.B. Modelling the rapid near-surface expansion of gas slugs in low-
477   viscosity magmas. *Geol. Soc. Spec. Publ.*   **2008**, *307*, pp. 147-167, DOI:10.1144/SP307.9

478   14. Del Bello, E.; Llewellin, E.W.; Taddeucci, J.; Scarlato, P.; Lane, S. J. An analytical model for gas overpressure
479   in slug-drive explosions: Insights into Strombolian volcanic eruptions. *J. Geophys. Res. Solid Earth.* **2012**, *117*,
480   DOI:10.1029/2011JB008747

481   15. Chouet, B.; Hamisevi, N.; McGetchi, T.R. Photoballistics of volcanic jet activity at Stromboli, Italy. *J.*
482   *Geophys. Res.* **1974**, *79*, pp. 4961-4976, DOI:10.1029/JB079i032p04961

483   16. McGonigle, A.J.S.; Aiuppa, A.; Ripepe, M.; Kantzas, E.P.; Tamburello, G. Spectroscopic capture of 1 Hz
484   volcanic SO_2 fluxes and integration with volcano geophysical data. *Geophys. Res. Lett.* **2009**, *36*,
485   DOI:10.1029/2009GL040494

486   17. Mori, T.; Burton, M. Quantification of the gas mass emitted during single explosions on Stromboli with the
487   SO_2 imaging camera. *J. Volcanol. Geotherm. Res.* **2009**, *188*, pp. 395-400, DOI:10.1016/j.volgeores.2009.10.005

488   18. Pering, T. D.; McGonigle, A.J.S.; James, M.R.; Tamburello, G.; Aiuppa, A.; Delle Donne, D.; Ripepe, M.
489   Conduit dynamics and post-explosion degassing on Stromboli: a combined UV camera and numerical
490   modelling treatment. *Geophys. Res. Lett.* **2016**, *43*, DOI:10.1002/2016GL069001.

491   19. Taddeucci, J.; Scarlato, P.; Capponi, A.; Del Bello, E.; Cimarelli, C.; Palladino, D.M.; Kueppers, U. High-
492   speed imaging of Strombolian explosions: The ejection velocity of pyroclasts. *Geophys. Res. Lett.* **2012**, *39*,
493   DOI:10.1029/2011GL050404

494   20. Taddeucci, J.; Alatorre-Ibarguengoitia, M.A.; Palladino, D.M.; Scarlato, P.; Camaldo, C. High-speed
495   imaging of Strombolian eruptions: Gas-pyroclast dynamics in initial volcanic jets. *Geophys. Res. Lett.* **2015**,
496   *42*, pp. 6253-6260, DOI:10.1002/2015GL064874

497   21. Delle Donne, D.; Ripepe, M.; Lacanna, G.; Tamburello, G.; Bitetto, M.; Aiuppa, A. Gas mass derived by
498   infrasound and UV cameras: Implications for mass flow rate. *J. Volcanol. Geotherm. Res.* **2016**, *325*, pp. 169-
499   178, DOI:10.1016/j.volgeores.2016.06.015

500   22. Kremers, S.; Lavallée, Y.; Hanson, J.; Hess, K.-U.; Chevrel, O.; Wassermann, J.; Dingwell, D.B. Shallow
501   magma-mingling-driven Strombolian eruptions at Mt. Yasur volcano, Vanuatu. *Geophys. Res. Lett.* **2012**, *39*,
502   DOI:10.1029/2012GL053312

23. Shinohara, H., Witter, J.B.; Volcanic gases emitted during mild Strombolian activity of Villarrica volcano, Chile. *Geophys. Res. Lett.* **2005**, *32*, DOI:10.1029/2005GL024131

24. Pering, T.D.; Tamburello, G.; McGonigle, A.J.S.; Aiuppa, A.; James, M.R.; Lane, S.J.; Sciotto, M.; Cannata, A.; Patane, D. Dynamics of mild strombolian activity on Mt. Etna. *J. Volcanol. Geotherm. Res.* **2015**, *300*, pp. 103-111, DOI:10.1016/j.volgeores.2014.12.013

25. Dalton, M. P.; Waite, G. P.; Watson, I. M.; Nadeau, P. A. Multiparameter quantification of gas release during weak Strombolian eruptions at Pacaya volcano, Guatemala, *Geophys. Res. Lett.* **2010**, *37*, DOI:10.1029/2010GL042617

26. Gaudin, D.; Taddeucci, J.; Scarlato, P.; Del Bello, E.; Ricci, T.; Orr, T.; Houghton, B.; Harris, A.; Rao, S.; Bucci, A. Integrating puffing and explosions in a general scheme for Strombolian-style activity. *J. Geophys. Res. Solid Earth.* **2017**, *122*, pp. 1860-1875, DOI:10.1002/2016JB013707

27. Gaudin, D., Taddeucci, J.; Scarlato, P.; Harris, A.; Bombrun, M.; Del Bello, E.; Ricci, T. Characteristics of puffing activity revealed by ground-based, thermal infrared imaging: the example of Stromboli Volcano (Italy). *Bull. Volcanol.* **2017**, *79*, DOI:10.1007/s00445-017-1108-x

28. James, M.R.; Lane, S.J.; Wilson, L.; Corder, S.B. Degassing at low magma-viscosity volcanoes: Quantifying the transition between passive bubble-burst and Strombolian eruption. *J. Volcanol. Geotherm. Res.* **2009**, *180*, pp. 81-88, DOI:10.1016/j.volgeores.2008.09.002

29. Bouche, E.; Vergniolle, S.; Staudacher, T.; Nercessian, A.; Delmont, J.-C.; Frogneux, M.; Cartault, F; Le Pichon, A. The role of large bubbles detected from acoustic measurements on the dynamics of Erta 'Ale lava lake (Ethiopia). *Earth Planet. Sci. Lett.* **2010**, *295*, pp. 37-48, DOI:10.1016/j.epsl.2010.03.020

30. Pering, T.D.; McGonigle, A.J.S.; James, M.R.; Capponi, A.; Lane, S.J.; Tamburello, G.; Aiuppa, A. The dynamics of slug trains in volcanic conduits: evidence for expansion driven slug coalescence. *J. Volcanol. Geotherm. Res.* **Under Review.**

31. Llewellin, E.; Del bello, E., Lane, S.J.; Capponi, A.; Mathias, S.; Taddeucci, J. Cyclicity in slug-driven basaltic eruptions: insights from large-scale analogue experiments. **2013,** In: EGU General Assembly, Vienna.

32. Llewellin, E.W.; Burton, M.R.; Mader, H.M.; Polacci, M. Conduit speed limit promotes formation of explosive 'super slugs'. **2014,** In: AGU Fall Meeting, San Francisco.

33. Kremers, S.; Wassermann, J.; Meier, K.; Pelties, C.; van Driel, M.; Vasseur, J.; Hort, M. Inverting the source mechanism of Strombolian explosions at Mt. Yasur, Vanuatu, using a multi-parameter dataset. *J. Volcanol. Geotherm. Res.* **2013**, *262*, pp. 104-122, DOI:10.1016/j.volgeores.2013.06.007

34. Mori, T.; Burton, M. The SO_2 camera: a simple, fast and cheap method for ground-based imaging of SO_2 in volcanic plumes. *Geophys. Res. Lett.* **2006**, *33*, DOI:10.1209/2006GL027916

35. Bluth, G.J.S.; Shannon, J.M.; Watson, I.M.; Prata, A.J.; Realmuto, V.J. Development of an ultra-violet digital camera for volcanic SO_2 imaging. *J. Volcanol. Geotherm. Res.* **2007**, 161, 47-56, DOI:10.1016/j.volgeores.2006.11.004

36. Kantzas, E.P.; McGonigle, A.J.S.; Tamburello, G.; Aiuppa, A.; Bryant, R.G. Protocols for UV camera volcanic SO_2 measurements. J. Volcanol. Geotherm. Res. **2010**, *194*, pp. 55–60, DOI:10.1016/j.jvolgeores.2010.05.003

37. Parfitt, E.A.; Wilson, L. Explosive volcanic eruptions – IX. The transition between Hawaiian-style lava fountaining and Strombolian explosive activity. *Geophys. J. Int.* **1995**, *121*, pp. 226-232, DOI:10.1111/j.1365-246X.1995.tb03523.x

38. Palma, J.L.; Calder, E.S.; Basualto, D.; Blake, S.; Rothery, D.A. Correlations between SO_2 flux, seismicity, and outgassing activity at the open vent of Villarrica volcano, Chile *J. Geophys. Res. Solid Earth.* **2008**, *113*, DOI:10.1029/2008JB005577

39. James, M.R.; Lane, S.J.; Houghton, B.F. *Unsteady explosive activity: strombolian eruptions.* In: Modeling Volcanic Processes: The Physics and Mathematics of Volcanism, eds. S.A. Fagents, T.K.P. Gregg, R.M.C. Lopes. pp. 107-129, **2013**

40. Manga, M. Waves of bubbles in basaltic magmas and lavas. *J. Geophys. Res.* **1996**, *101*, pp. 17,457-17,465, DOI:10.1029/96JB01504

41. Herd, R.A.; Pinkerton, H. Bubble coalescence in basaltic lava: Its impact on the evolution of bubble populations. *J. Volcanol. Geotherm. Res.* **1997,** *75*, DOI:10.1016/S0377-0273(96)00039-X

42. Harris, A.J.L.; Dehn, J.; Calvari, S. Lava effusion rate definition and measurement: a review. *Bull. Volcanol.* **2007,** 70, pp. 1-22, DOI:10.1007/s00445-007-0120-y

43. Llewellin, E.W.; Del Bello, E.; Taddeucci, J.; Scarlato, P.; Lane, S.J. The thickness of the falling film of liquid around a Taylor bubble. *Proc. Royal. Soc. A.* **2012**, *468*, DOI:10.1098/rspa.2011.0476

557 44. Viana, F.; Pardo, R.; Yánez, R.; Trallero, J.L.; Joseph, D.D.. Universal correlation for the rise velocity of long
558   gas bubbles in round pipes. *J. Fluid Mech.* **2003,** *494,* pp. 379-398, DOI:10.1017/S0022112003006165

559 45. Campos, J.B.L.M.; Guedes de Carvalho, J.R.F. An experimental study of the wake of gas slugs rising in
560   liquids. *J. Fluid Mech.* **1988,** *196*, pp. 27-37, DOI:10.1017/S0022112088002599

561 46. Pinto, A.M.F.R.; Campos, J.B.L.M. Coalescence of two gas slugs rising in a vertical column of liquid. *Chem.*
562   *Eng. Sci.* **1996,** *51*, pp. 45-54, DOI:10.1016/0009-2509(95)00254-5

563 47. Joseph, D.D. Rise velocity of a spherical cap bubble. *J. Fluid Mech.* **2003,** *488,* pp. 213-223,
564   DOI:10.1017/S0022112003004968

565 48. Komasawa, I.; Otake, T.; Kamojima, M. Wake behaviour and its effect on interaction between spherical-cap
566   bubbles. *J. Chem. Eng. Japan.* **1980,** *13*, pp. 103-109, DOI:10.1252/jcej/13/103

567 49. Corsaro, R.A.; Pompilio, M. *Dynamics of Magmas at Mount Etna, in Mt. Etna: Volcano Laboratory* (eds A.
568   Bonaccorso, S. Calvari, M. Coltelli, C. Del Negro and S. Falsaperla), American Geophysical Union,
569   Washington, D. C. **2004,** DOI: 10.1029/143GM07

570 50. Vergniolle, S.; Brandeis, G. Strombolian explosions: 1. A large bubble breaking at the surface of a lava
571   column as a source of sound. *J. Geophys. Res.* **1996,** 101, pp. 20,433–20,447, DOI:10.1029/96JB01178.

572 51. Métrich, N.; Bertagnini, A.; Landi, P.; Rosi, M. Crystallization driven by decompression and water loss at
573   Stromboli volcano (Aeolian Islands, Italy), *J. Petrol.* **2001,** *42,* pp. 1471–1490,
574   DOI:10.1093/petrology/42.8.1471

575 52. Vergniolle, S.; Brandeis, G.; Mareschal, J.C. Strombolian explosions 2. Eruption dynamics determined from
576   acoustic measurements. *J. Geophys. Res.* **1996,** *101,* pp. 20,449–20,466, DOI:10.1029/96JB01925.

577 53. Harris, A.J.L.; Stevenson, D.S. Thermal observations of degassing open conduits and fumaroles at
578   Stromboli and Vulcano using remotely sensed data. *J. Volcanol. Geotherm. Res.* **1997,** *76,* pp. 175–198,
579   DOI:10.1016/S0377-0273(96)00097-2

580 54. Delle Donne, D.; Ripepe, M. High-frame rate thermal imagery of Strombolian explosions: Implications for
581   explosive and infrasonic source dynamics. *J. Geophys. Res. Solid Earth.* **2012,** *117*, DOI:10.1029/2011JB008987

582 55. Krishna, R.; Urseanu, M.I.; van Baten, J.M.; Ellenberger, J. Rise velocity of a swarm of large gas bubbles in
583   liquid. *Chem. Eng. Sci.* **1999,** *54*, pp. 171-183, DOI:10.1016/S0009-2509(98)00245-0

584 56. Mayor, T.S.; Pinto, A.M.F.R.; Campos, J.B.L.M. Vertical slug flow in laminar regime in the liquid and
585   turbulent regime in the bubble wake – Comparison with fully turbulent and fully laminar regimes. *Chem.*
586   *Eng. Sci.* **2008,** *63*, pp. 3614-3631, DOI:10.1016/j.ces.2008.04.020

587 57. Mayor, T.S.; Pinto, A.M.F.R.; Campos, J.B.L.M. On the gas expansion and gas hold-up in vertical slugging
588   columns – A simulation study. *Chem. Eng. Prog.* **2008,** *47,* pp. 799-815, DOI:10.1016/j.cep.2007.01.031

589 58. Chouet, B.; Dawson, P.; Ohminato, T.; Martini, M.; Saccorotti, G.; Giudicpietro, F.; De Luca, G.; Milana, G.;
590   Scarpa, R. Source mechanisms of explosions at Stromboli Volcano, Italy, determined from moment-tensor
591   inversions of very-long period data. *J. Geophys. Res.* **2003,** *108*, DOI:10.1029/2002JB001919

592 59. James, M.R.; Lane, S.J.; Chouet, B.; Gilbert, J.S. Pressure changes associated with the ascent and bursting of
593   gas slugs in liquid-filled vertical and inclined conduits. *J. Volcanol. Geotherm. Res.* **2004,** *129,* pp. 61-82,
594   DOI:10.1016/S0377-0273(03)00232-4

595 60. Capponi, A.; James, M.R.; Lane, S.J. Gas slug ascent in a stratified magma: Implications of lfow organisation
596   and instability for Strombolian eruption dynamics. *Earth Planet Sci. Lett.* **2016,** *435,* pp. 159-170,
597   DOI:10.1016/j.epsl.2015.12.028

598 61. McGonigle, A.J.S.; Pering, T.D.; Wilkes, T.C.; Tamburello, G.; D'Aleo, R.; Bitetto, M.; Aiuppa, A. Ultraviolet
599   imaging of volcanic plumes: a new paradigm in volcanology. *Geosciences.* **2017,** *7,*
600   DOI:10.3390/geosciences7030068

601 62. Aiuppa, A.; Federico, C.; Paonita, A.; Giudice, G.; Valenza, M. Chemical mapping of a fumarolic field: La
602   Fossa Crater, Vulcano Island (Aeolian Islands, italy). *Geophys. Res. Lett.* **2005,** *13,*
603   DOI:10.1029/2005GL023207

604 63. Shinohara, H. A new technique to estimate volcanic gas composition: plume measurements with a portable
605   multi-sensor system. *J. Volcano. Geotherm. Res.* **2005,** *143,* pp. 319-333, DOI:10.1016/j.volgeores.2004.12.004

606 64. Allard, P.; Burton, M.; Muré, F. Spectroscopic evidence for a lava fountain driven by previously
607   accumulated magmatic gas. *Nature.* **2005,** *433,* pp. 407-410, DOI:10.1038/nature03246

608 65. Aiuppa, A.; Moretti R.; Federico C.; Giudice G.; Gurrieri S.; Liuzzo M.; Papale P.; Shinohara H.; Valenza M.
609   Forecasting Etna eruptions by real-time observation of volcanic gas composition. *Geology.* **2007,** *35*, pp.
610   1,115–1,118, DOI: 10.1130/G24149